# Laser spectroscopy of gas confined in nanoporous materials

Svensson, Tomas; Shen, Zhijian

*Published in:*
Applied Physics Letters

*DOI:*
10.1063/1.3292210

2010

# Contents

# Chapter 1

# Introduction

## 1.1 Background

In 2001, Sjöholm *et al.* published an article on the analysis of gas inside scattering media by the use of tunable diode laser absorption spectroscopy [1]. This was the first time the GASMAS method (gas in scattering media absorption spectroscopy) was mentioned. Since then, the technique has been used for a long line of applications. The GASMAS technique can be used to study diffusion properties in different materials, for example wood and fruits [2, 3]. The porosity of pharmaceutical tablets could be measured by studying the GASMAS signal and correlating it with time-of-flight spectroscopy. Drying processes of wood have been studied [4]. A number of medical applications have been developed, for example measurements on the concentration of oxygen in the sinuses for diagnostic purposes [5]. There have also been feasibility studies to find out if it is possible to monitor the oxygen concentration in the lungs of premature neonates, with positive outcome [6]. Non-intrusive measurements of food packages constitute another application that has been studied [7]. A review for the GASMAS technique can be found in [8].

In the very first article on GASMAS [1], there was a sentence mentioning expected additional wall-collision broadening in the case when gas was confined in very small pores:

> "In the limit of very small (nanometer-scale) enclosures of free gas, additional collisional broadening and shifts of diagnostic value can be expected."

The wall collision broadening has previously been studied in the case of microwave spectroscopy at very low pressures [9, 10, 11]. In this regime it has been shown, theoretically and experimentally, that there is an additional line broadening effect due to molecular collisions with the walls of the container, and that this broadening effect can be observed when the mean free path length of the molecules is comparable to the size of the container. In these articles, this was achieved by measuring at very low pressures with gas cells of the centimeter range. When performing GASMAS measurements on scattering samples with nanometer-sized pores, the mean free path length of the molecules at atmospheric pressures is comparable with the size of the pores. This gives a great

opportunity to study the line-broadening mechanism closer, which has been done in [12, 13].

The wall-collision broadening is a quite unknown effect in molecular spectroscopy, and has not been examined very much. The line shape of the absorption lines due to wall collision is not a Lorentzian function or a Gaussian, which is the result of the pressure and Doppler broadening, but some other unknown line shape. The physics of the line-broadening effect due to wall-collisions is thus different compared to broadening due to collisions between molecules (pressure broadening). The effect is extremely interesting from a physical point of view, but there may also, in the future, be applications to the method. For example, the method may be used to measure the pore size distribution in nanoporous materials.

## 1.2 Scope

The primary goal of this work was to study the line-broadening mechanism of absorption lines of gas that is confined in nanoporous materials. Another goal was to try to perform GASMAS measurements on carbon dioxide inside heavily scattering ceramics. A setup for measuring GASMAS on the molecular oxygen already existed when this diploma project began. A few modifications to this setup were performed. For instance, the program for sampling and analyzing measurement data was modified to automatically stop the averaging process when the resulting averaged signal was good enough, and the gas control system was modified so that the chamber could be filled with other gases than air, for example $N_2$ or pure $O_2$. A setup for measuring on water vapor in ceramics was built, but unfortunately, the laser broke before any measurements could be performed. Another setup was built to measure on $CO_2$, and preliminary measurements have been performed on $CO_2$ in polystyrene foam and porous ceramics.

## 1.3 Outline

This report is divided into nine chapters: Introduction, absorption spectroscopy, tunable diode laser absorption spectroscopy (TDLAS), gas in scattering media absorption spectroscopy (GASMAS), instrumentation, pressure dependence investigation, measurements, discussion and summary.

Chapter 2 describes the basics of absorption spectroscopy. The structure of the energy level diagram is discussed, then the Beer-Lambert law is presented, and, finally, the line shape of absorption lines and different broadening mechanisms are discussed. In chapter 3, the basics of TDLAS, which is a specific type of absorption spectroscopy, is presented. There is also a section about diode lasers, which constitute a vital component in TDLAS, and about different types of diode lasers and their advantages and disadvantages. Then, in chapter 4, the GASMAS method is discussed. This is a special type of TDLAS, which studies gas inside scattering media using TDLAS. The focus of this chapter is on GASMAS performed on nanoporous ceramics.

After the chapters about the basic theory of the methods used in the diploma project, chapter 5 describes the instrumentation that has been used in the ex-

perimental work. First, three different setups for measuring on $O_2$, $H_2O$, and $CO_2$, separately, are described. Then, there is a description of the gas control system. After that, the results from system performance verification measurements on the setup for $O_2$ are presented. Finally, there is a description of the program for automatic determination for the number of averages during the measurement process, and the results of these measurements.

In chapter 6, measurements are performed on macroporous materials, to make sure that the extra line broadening that can be seen at low pressures is due to wall-collision broadening and not to some other line broadening effect or instrumental factor of the system. When measuring on polystyrene foam, it became apparent that the diffusion of gas out of polystyrene foam is slow. This lead to measurements on the diffusion of gas out of polystyrene foam at low pressures. Then, measurements are performed on a macroporous material with fast diffusion to check the line shape at low pressures.

Chapter 7 shows the results of the measurements on line broadening of $O_2$ in nanoporous zirconia. Then the results of the GASMAS measurements on the $CO_2$ in polystyrene foam and porous ceramics are presented. In chapter 8, the results of the measurements are discussed. Finally, chapter 9 summarizes the report and suggests future work that could be performed extending the present work.

# Chapter 2

# Absorption spectroscopy

This chapter will describe the basics of absorption spectroscopy. First, there is a section describing the structure of the energy level diagram in molecules. To simplify the derivations, the description will be concentrated on a diatomic molecule. After that, there will be a part about transition rules between different states in the energy level diagram. Next, the basics of the Beer-Lambert law will be explained. This law relates a connection between the strength of the absorption of light, the concentration of absorbing molecules and the length of the absorption path and is the most common method for analyzing absorption signals. Finally, there is a section on the broadening of absorption lines due to temperature, pressure and wall collisions.

## 2.1 Molecular structure

The energy levels of an atom depend on a multitude of things, but the largest contribution comes from the configuration of the electrons. A molecule is formed when two or more atoms are bound together. The energy level diagram of a molecule is much more complicated than that of an atom, since in addition to the energy arising from different electronic configurations, the different nuclei in a molecule can rotate and vibrate with respect to each other. The first step when trying to analyze molecular energy levels is the so-called Born-Oppenheimer approximation. This approximation says that since the nuclei of the atoms are much heavier than the electrons and move much slower, they can be assumed to be fixed when considering the electronic movements [14]. This means that the total energy of the molecule can be assumed to be equal to the sum of the the energy due to electronic configurations and the rotational and vibrational energy of the nuclei, according to equation (2.1) [15].

$$E_{\text{total}} = E_{\text{electronic}} + E_{\text{vibrational}} + E_{\text{rotational}} \tag{2.1}$$

The largest energy contribution comes from the electronic configurations. Energy levels with different electronic configurations are normally separated by a few eV, which gives rise to transition in the visible-UV range. For each electronic configuration, there are a number of rather closely situated energy levels corresponding to different vibrational states of the nuclei. The separation between different vibrational states is around 0.1 eV, corresponding to transitions

in the IR region. The vibrational states are in their turn split into closely spaced levels corresponding to different rotational energy of the nuclei, which are separated by a few meV, which gives transitions at frequancies in the microwave regime. This means that the structure of the energy level diagram will look something like in Figure 2.1.

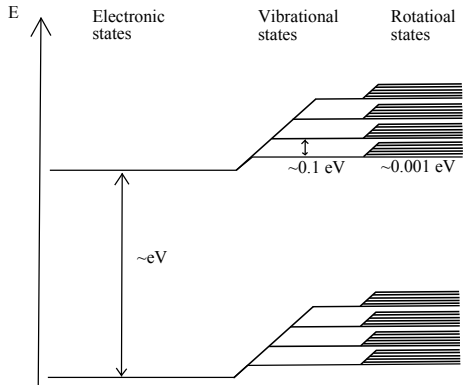


Figure 2.1: *Schematic of the energy level structure of a diatomic molecule. The electronic states are divided into many smaller vibrational levels, which are in turn divided into many smaller rotational levels.*

The theory for the energy levels of a molecule becomes much more complicated for polyatomic molecules. In this section, the theory for the energy level diagram of a diatomic molecule will be described. The energy level structure of polyatomic molecules is described in [15].

### 2.1.1 Electronic states

The configuration of the electrons of a molecule is a large contribution to the energy of the molecule. The energy arising from the electronic configurations in a molecule is mostly dependent on the distance of the electrons from the nuclei. Furthermore, there are also energy contributions from the orbital angular momentum and the spin of the electrons [15].

In atoms, the electrons move in an electric field from the nucleus which is spherically symmetric, and the orbital angular momentum, $L$, is a constant of motion. In a diatomic molecule, there is a cylindrical symmetry instead, which means that the projection of the angular momentum on the symmetry axis, which is represented by the quantum number $M_L$, will be a constant of motion. It can be shown that states with different $|M_L|$-values will have different energies [14]. This gives the basic energy of the electronic states of a molecule. The states are denoted with $\Lambda$ as

$$\Lambda = |M_L| = 0(\Sigma), 1(\Pi), 2(\Delta), 3(\Phi), ... \tag{2.2}$$

The states with $|M_L| > 0$ have a double degeneracy, since, e.g., the states with $M_L = \pm 1$ have the same energy. If there are more than one electron, the total $M_L$-value for these electrons is given by the absolute value of the sums of the different $M_L$ values [15].

To characterize the electronic state, the spin of the electrons also needs to be considered. As was the case for the orbital angular momentum, the projection of the total spin on the symmetry axis, $M_S$ (denoted with $\Sigma$), will be a constant of motion and can have $2S + 1$ values.

The projection of the total angular momentum of the electrons on the symmetry axis, normally called $\Omega$, is given by $\Omega = |\Lambda + \Sigma|$. Since $\Lambda$ and $\Sigma$ point in either the same or opposite directions along the symmetry axis, $\Omega$ is either the sum or the modulus of the difference between $\Sigma$ and $\Lambda$.

### 2.1.2 Vibrational energy

The potential energy of a diatomic molecule depends on the distance $r$ between the nuclei. A simplified explanation of the energy is that the nuclei are attracted by the electrons around the other nuclei, but if the nuclei are too close, they will repel each other. The potential energy for the nuclei at different distances from each other can be described by a Morse potential; see equation (2.3). Here $E$ is the potential energy, $D_\mathrm{e}$ the dissociation energy of the molecule, $a$ is a constant, different for different molecules, and $r_\mathrm{eq}$ is the equilibrium distance of the nuclei, which is the distance where the energy of the molecule is minimized.

$$E = D_\mathrm{e}(1 - e^{-a(r-r_\mathrm{eq})})^2 \tag{2.3}$$

The nuclei of the molecule will vibrate with respect to each other around the equilibrium distance. For lower vibrational energies, the Morse potential can be approximated with a harmonic oscillator potential; see Figure 2.2. This means that the energy of the vibration will be the given by the energies of a harmonic oscillator, according to equation (2.4).

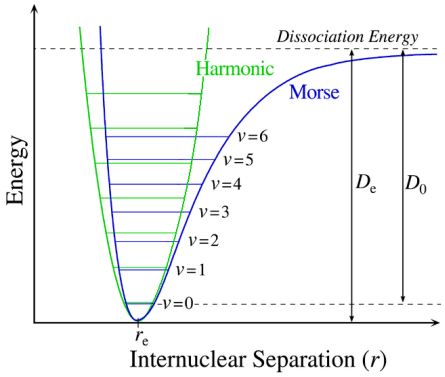


Figure 2.2: *The Morse potential, approximated with a harmonic oscillator. The energy levels of the different vibrational states are drawn in the potential, both for the Morse potential and the harmonic oscillator approximation (modified from [16]).*

$$E_v = (v + 1/2)h\nu_\mathrm{c} \tag{2.4}$$

Here $E$ is the vibrational energy, $\nu_\mathrm{c}$ is the vibrational frequency, $h$ is Planck's constant and $v = 0, 1, 2...$ is a positive integer. For higher vibrational levels, the harmonic oscillator is not a good approximation and the vibrational energy of the molecule will be lower than the energy predicted by the harmonic oscillator.

### 2.1.3 Rotational energy

The nuclei of a molecule can also rotate around their common centre of mass, which will give an energy contribution to the total energy of the molecule. In this derivation of the rotational energy, a rigid rotator consisting of two nuclei with different mass will be assumed. The nuclei have the masses $m_1$ and $m_2$ and their respective distances to the centre of gravity are $r_1$ and $r_2$. This gives the nuclei a moment of inertia $I = \mu r^2$, where $\mu = m_1 m_2/(m_1 + m_2)$ is the reduced mass and $r = r_1 + r_2$ is the distance between the molecules.

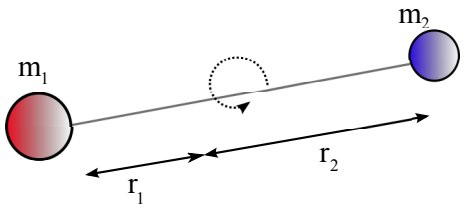


Figure 2.3: *In a diatomic molecule, the nuclei can rotate around their common centre of mass*

It can be shown that the energy of a rigid rotating diatomic molecule is given by equation (2.5) [15].

$$E = BJ(J+1), \qquad \text{where } B = \hbar^2/(2I), \qquad J = 0, 1, 2, \ldots \tag{2.5}$$

If the rotation of the nuclei cannot be described as rigid, the distance between the molecules will increase as the molecule rotates faster, causing the moment of inertia, $I$, to increase. This means that the rotational energy will decrease in the higher rotational states for an elastic rotator compared to the levels of a rigid rotator. The energy will instead be given by equation (2.6).

$$E = BJ(J+1) - DJ^2(J+1)^2, \tag{2.6}$$

where the centrifugal distortion constant $D \ll B$ is a positive constant.

### 2.1.4 Combined rotational and vibrational energy

The energy of a vibrational-rotational state is given by equation (2.7).

$$E = (v + 1/2)h\nu_c + BJ(J+1) \tag{2.7}$$

The vibration of the nuclei will affect the moment of inertia of the rotation. This means that the rotational constant $B$ will be different in different vibrational states. For vibrational-rotational levels in the same electronic state, the rotational constant will be lower in the higher vibrational levels.

## 2.2 Transition rules

A molecule can make a transition from one energy level to another by absorbing or emitting light with the same energy as the difference in energy between

the levels. The most common type of transitions is called electric dipole transitions, where the transition happens by interaction between the molecule and the electric field of the light.

Transitions can happen between different electronic, vibrational and rotational energy levels. It is not possible to make a transition between all energy levels by electric dipole transitions. There are special rules determining the transitions that are allowed. In this section, the case of transitions between different vibrational and rotational levels within a certain electronic state will first be described. After that, transitions between different electronic states will also be considered.

Magnetic dipole transitions are of a different type, where the interaction is with the magnetic field of the light. This type of transition has different transition rules than electric dipole transitions, and is normally weaker.

### 2.2.1 Vibrational-rotational spectra

Molecules can absorb or emit radiation when changing from one vibrational state to another. At the bottom of the Morse potential, where the harmonic oscillator approximation is valid, the selection rule is $\Delta v = \pm 1$. At higher levels, when the harmonic oscillator is not such a good approximation, it is also possible to have transitions with $\Delta v = \pm 2, \pm 3$, etc.

Light is also emitted when a molecule changes from one rotational state to another. It can be shown, both classically and by quantum mechanics, that an atom or a molecule can only absorb or emit light if its electric dipole moment is changed. Because of this, the selection rule for transitions between different rotational levels is $\Delta J = \pm 1$.

Often, a transition between two vibrational levels is also accompanied by a change in the rotational energy as well. Since the rotational constant is different in different vibrational levels, this must be taken into account when calculating the energy of the transition. The rotational constant in the upper vibrational level will be called $B'$ and the constant in the lower level $B''$.

With the selection rules for vibrational and rotational transitions, $\Delta v = \pm 1$ and $\Delta J = \pm 1$, the energy for a transition between different rotational-vibrational state is given by equation (2.8). Transitions to different rotational states gives that the spectrum will be divided into two so-called branches, the R-branch (for $\Delta J = +1$)and the P-branch (for $\Delta J = -1$).

$$\Delta E = h\nu_c \begin{cases} +2B' + (3B' - B'')J + (B' - B'')J^2 & J \to J+1 \quad J = 0, 1, \dots \\ -(B' + B'')J + (B' - B'')J^2 & J \to J-1 \quad J = 1, 2, \dots \end{cases} \tag{2.8}$$

These rather long and complicated equations can be merged into a single equation by introducing a new number $m$ instead of $J$. The energy of the transitions is then given by equation (2.9).

$$\Delta E = h\nu_c + (B' + B'')m + (B' - B'')m^2 \begin{cases} m = 1, 2, 3, \dots & R - branch \\ m = -1, -2, -3, \dots & P - branch \end{cases} \tag{2.9}$$

The relative population on different vibrational levels is governed by the

Boltzmann distribution (2.10).

$$\frac{N_1}{N_2} = \frac{g_1}{g_2} e^{-\Delta E/kT}, \tag{2.10}$$

where $N_1$ and $N_2$ are the populations on each level, $g_1$ and $g_2$ are the statistical weight of each level, $\Delta E$ is the energy difference between the levels, $k$ is Boltzmann's constant and $T$ is the temperature. Because of this, the R-branch in vibrational-rotational transitions will have a little higher intensity compared with the P-branch. Figure 2.4 shows the R- and P-branches for CO.

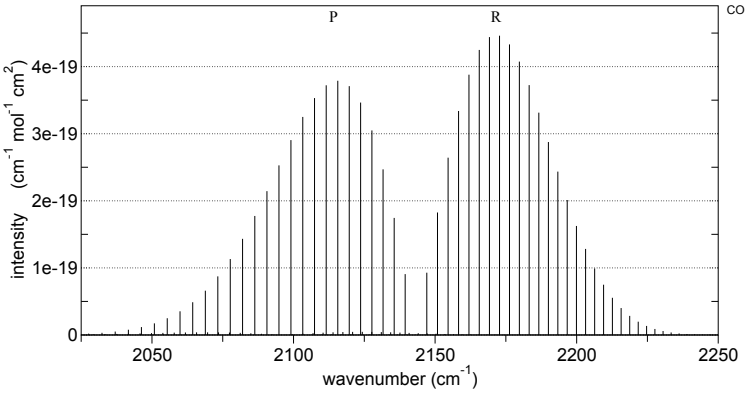


Figure 2.4: *The R-and-P branches for CO for rotational-vibrational transitions [17].*

### 2.2.2 Electronic transitions

Since the spacing between different electronic levels is much larger than between vibrational levels, transitions between different electronic configurations have much shorter wavelengths, typically in the visible or UV region. These transitions can be combined with transitions between different vibrational/rotational levels.

The intensity of the transitions is governed by the *Franck-Condon principle*. This states that the electronic transition happens so quickly that the vibrating nuclei do not change their internuclear distance during that time. This means that between some levels, transitions to the vibrational state $v = 0$ will have the largest intensity, while for others levels transitions to another $v$ might be more likely (for more detailed explanations, please read [15]).

Since the molecule must change its electric dipole moment during a transition, the electronic states for which the transitions occur influence the allowed vibrational/rotational transitions which can occur. If the electronic states involved have no angular momentum, the selection rules for the vibrational/rotational transitions are the same as for transitions within an electronic state. This will give the R-and-P branches in the electronic transition as well. If the transition is between states with different angular momentum, there will also be a Q-branch, which corresponds to transitions with $\Delta J = 0$.

## 2.3 Beer-Lambert law

A gas containing a certain type of molecules will absorb light at different wavelengths according to its energy levels diagram and the transition rules between different levels. If light of a resonance wavelength for a certain molecule is sent through a gas containing these molecules, the light will be absorbed. The intensity of the light will then decrease as it passes through the gas. The decrease is governed by the Beer-Lambert law

$$I = I_0 e^{-\sigma(\nu)NL} \tag{2.11}$$

where $I_0$ is the intensity before passing through the gas, $I$ is the intensity after the gas, $\sigma(\nu)$, is the cross-section of the absorption, $\nu$ is the frequency of the light, $N$ is the concentration of molecules in the gas and $L$ is the length that the light passes through the gas. The Beer-Lambert law also works for the absorption of light in liquids and solids.

As can be seen in equation (2.11), the amount of light that is absorbed depends on the cross-section for absorption, the concentration of the gas and the length of the absorption path length. The cross-section has maximum values at the frequencies when transitions are possible, according to the energy level diagram and the selection rules, as was explained in the previous section. However, the cross-section has a small width around these resonance frequencies, which will be studied in the next section.

## 2.4 Lineshapes

In the previous sections the wavelengths at which a molecule absorbs light has been explained. This has been shown to be a discrete spectrum, with the molecule absorbing at only one wavelength in an interval and none near it. In reality, the wavelength at which a molecule absorbs is not infinitely sharp, but has a certain shape and width centered around the resonance frequency. This section will go through some common types of factors that cause a broadening of the absorption lines. The type of broadening that determines the line shape of the absorption lines depends on the environment around the absorbing molecules.

### 2.4.1 Natural broadening

The most fundamental line broadening mechanism, which only depends on the molecules themselves and not on the surrounding environment, is the *natural line broadening*. According to Heisenberg's uncertainty principle, $\Delta\nu \cdot \Delta t \geq 1/2\pi$, an energy level that does not have infinite lifetime cannot be infinitely sharp in energy [15]. This gives a natural broadening of the transitions to a state with the lifetime $\tau$. The line shape, $g(\nu)$, of the absorption line from the natural broadening is a Lorentzian curve; see equation (2.12), with a line width given by $\Delta\nu = 1/2\pi\tau$.

$$g(\nu) = \frac{\Delta\nu/2\pi}{(\nu - \nu_0)^2 + (\Delta\nu/2)^2} \tag{2.12}$$

The natural broadening is often very small and negligible compared with the other types of broadening of a spectral line, like pressure broadening and Doppler broadening.

### 2.4.2 Pressure broadening

In a gas, the molecules can collide with each other. These collisions both shorten the lifetime of the upper level of the molecule, thereby increasing the broadening of the absorption line, and also introduce a random phase shift in the wave function, which also increases the line width. The line shape of this so-called *pressure broadening* is Lorentzian. The collision rate depends on the pressure, giving a broader line for higher pressures.

The pressure broadening is called a homogeneous broadening, since it affects all molecules in the gas in the same way. The natural broadening is also homogeneous. A broadening effect that is inhomogeneous is the Doppler broadening.

### 2.4.3 Doppler broadening

The molecules in a gas at a given temperature move around with different velocities. The velocities of the molecules in the gas follow the Maxwell distribution given by equation (2.13), where $v$ is the velocity of the molecules in the gas, $M$ is the molecular weight, $R$ is the general gas constant and $T$ is the temperature.

$$f(v) = \sqrt{\frac{M}{2\pi RT}} e^{-\frac{M}{2RT}v^2} \tag{2.13}$$

Since the molecules are moving, light that comes towards them in a certain direction will be Doppler shifted (see Figure 2.5).

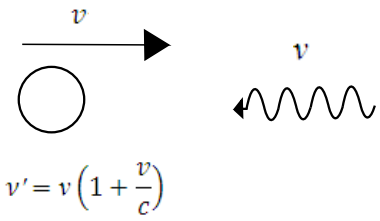


Figure 2.5: *The molecule moving towards the light with velocity sees a higher frequency* $\nu' = \nu(1 + v/c)$ *than the actual frequency of the light.*

Because of the Doppler shift, the molecules in the gas can absorb light at other frequencies that are shifted slightly from the resonance frequency. Since all atoms move with different speed and in different directions, the result is that light will be absorbed in an interval around the resonance frequency. The line is said to be Doppler broadened. Naturally, the Doppler broadening depends on the velocity distribution in the gas. It can be shown that the line shape, $g(\nu)$, of a Doppler broadened line is a Gaussian curve, according to equation (2.14).

$$f_D(\nu) = \frac{\sqrt{\ln 2}}{\sqrt{\pi}\Delta\nu_D} e^{-\ln 2(\nu/\Delta\nu_D)^2} \tag{2.14}$$

Here $\Delta\nu_D$ is the width of the absorption line and is given by equation (2.15).

$$\Delta\nu_D = \frac{2\sqrt{2R\ln 2}}{c}\nu_0\sqrt{\frac{T}{M}} \tag{2.15}$$

The Doppler broadening is an inhomogeneous broadening, since it is caused by all atoms absorbing at slightly different frequencies. The Doppler broadening depends on the temperature and the molecular weight and on the frequency of the transition. For transitions in the near-IR and relatively light molecules (like $O_2$ and $H_2O$) at room temperature and atmospheric pressure, the pressure broadening is normally the most dominating broadening effect and the line shape is approximately Lorentzian. For lower pressures, when the Doppler broadening and the pressure broadening are equally strong, the line shape is a Voigt profile, which is a convolution of a Gaussian and Lorentzian function.

### 2.4.4 Wall collision broadening

If a gas is confined in a container, the molecules will collide with the walls of this container. These collisions also affect the width of the absorption lines. Normally, in a large container and at atmospheric pressures, the mean free path of the molecules before they collide with other molecules is much smaller than the distance between the walls of the container, and the broadening due to collisions with the walls will be negligible compared to other broadening effects.

In [9], the effect of wall-collision broadening was observed for microwave lines at pressures of some milli-Torr. The low pressure rendered the mean free path length of the molecules comparable with the size of the gas cell, making it possible to observe the wall-collision broadening. The broadening was calculated theoretically and was found to depend on the shape of the cell. Assuming a cell consisting of two infinite parallel planes, a formula for the wall-collision broadening was determined. This calculation was improved in [10], and the calculations were also performed for a cylindrical container. It was found that the line shape of the absorption lines is not Lorentzian and that the line width due to wall collisions could be described by equation (2.16).

$$\Delta\nu = \frac{Q}{L}\sqrt{\frac{2kT}{m}} \tag{2.16}$$

where $k$ is the Boltzmann constant, $T$ is the temperature of the gas, $m$ is the mass of the molecules, $L$ is the length of the absorption cell and $Q$ is a constant that can be calculated numerically. Experimental values were found to agree with this theory.

In [11], calculations were performed to estimate the total width due to both intermolecular collisions and wall collisions. It was found that the line width could be calculated by the formula presented in equation (2.17),

$$\Delta\nu = \Delta\nu_{\text{mol}} + r_0(r)\Delta\nu_{\text{wall}} \tag{2.17}$$

where $\Delta\nu$ is the line width arising from both intermolecular collisions, $\Delta\nu_{\text{mol,wall}}$ is the line width due to intermolecular collisions and wall collisions separately, $r = \Delta\nu_{\text{mol}}/\Delta\nu_{\text{wall}}$ and $r_0(r)$ is a scaling factor that can be calculated theoretically. For small values of $r$, i.e. when the wall collision broadening is comparable with the pressure broadening, the line shape was found to differ from a Lorentzian curve.

Wall-collision broadening has also been observed when a gas is confined in nanoporous materials [12, 13]. This will be discussed in the chapter on GASMAS.

# Chapter 3

# Tunable diode laser absorption spectroscopy

A common way to perform absorption spectroscopy is to shine laser light on a gas and then sweep the wavelength of the laser over the absorption line of the gas. Then the decrease in transmitted intensity through the gas when the laser is tuned to the absorption wavelength is measured. Diode lasers are ideal for this task since it is easy to alter the wavelength by changing the driving current to the laser. The use of diode lasers for absorption spectroscopy has been given the name "Tunable diode laser absorption spectroscopy" (TDLAS). This chapter starts by going through the basic principles of TDLAS. Then, the Fabry-Pérot etalon is described, and in relation to this, the problem of unwanted interference fringes will be discussed. Finally, there is a section about the basic principles and different types of diode lasers.

## 3.1 Principles of TDLAS

A diode laser achieves population inversion by driving a forward current through a p-n junction. The output wavelength of a laser diode can be tuned over a certain range of wavelengths by changing the temperature and/or the driving current to the diode. The temperature is mostly used to set the laser to roughly the correct wavelength, while the current is used to sweep the wavelength repeatedly over the absorption line of the molecule to be studied.

The output power also changes when the driving current is modulated. Therefore, the detected light intensity will be a ramp, where different points in the sweep correspond to different wavelengths as well as different intensities. When the light passes the resonance wavelength, the intensity of the transmitted light decreases; see Figure 3.1.

The transmitted light is related to the incoming light by the Beer-Lambert law (2.11), which was described in the chapter on absorption spectroscopy. Here, $I_0$ is the intensity of the light without any absorbing molecules, which may be found by fitting a polynomial to the transmitted intensity outside of the absorption dip. The absorption is then found by dividing the signal with the baseline; see Figure 3.1.

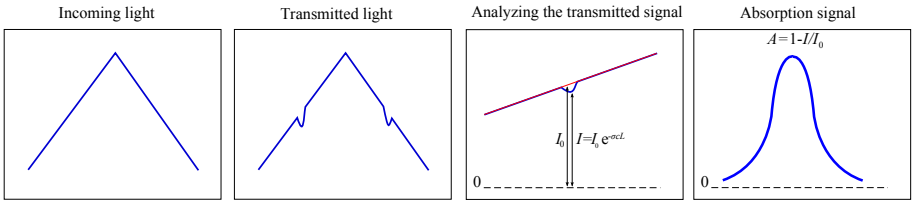


Figure 3.1: *The principles of analyzing an absorption signal with TDLAS. Left: The laser output power as a function of time during one sweep of the driving current. Each point on the slope corresponds to a different frequency of the laser light. Middle left: The light intensity transmitted through the sample decreases when the laser is at the resonance frequency. Middle right: The transmitted signal is analyzed with the Beer-Lambert law. The red line is the baseline found by fitting a polynomial to the signal. Right: The absorption signal.*

The advantages with TDLAS are many compared with other types of absorption spectroscopy. Diode lasers are small and compact and relatively inexpensive, compared with other tunable laser light sources. They can be made to have single-mode operation and narrow linewidths. It is easy to sweep the wavelength of the laser by applying a ramped current, and if weak signals are to be studied, a faster modulation can be added to the wavelength by modulating the driving current to the laser. Wavelength modulation techniques have been discussed in for example [18], [19] and [20], and will not be discussed here.

The disadvantages of TDLAS are mainly that there is a limited choice of wavelength range, and that the tuning range is relatively small. A laser diode can normally only be tuned a few nm, which is troublesome if many absorption lines are to be studied quasi-simultaneously. There are still no diode lasers in the UV-region (ultra-violet), and diodes in the mid-IR-and-IR regions normally need powerful cooling to work.

## 3.2 Fabry-Pérot etalon

A Fabry-Pérot-etalon is a useful tool for frequency calibration in TDLAS. It normally consists of a glass plate with two parallel, highly reflective surfaces. Because of this, light that passes through the etalon will undergo multiple reflectance, and the light will pass many times through the etalon. This is illustrated in Figure 3.2. The light is both transmitted and reflected in each surface. The reflected beams are drawn beside the transmitted beams to show the effect more clearly (in reality, all beams pass on top of each other).

After the etalon, the light that passed straight through the etalon will interfere with the light that was transmitted after a number of reflections. If the light that is transmitted through the etalon is in phase, the transmission of light will be high due to constructive interference. This will happen for waves that can fit an integer number of half wavelengths in the etalon length $L$. Since there are many wavelengths that fulfil this condition, the transmittance of light through the etalon will vary periodically if the frequency of the laser light is scanned over a frequency interval. The frequency difference between two adjacent wavelengths that have high transmittance is called the *free spectral range*, $\Delta\nu_{\mathrm{FSR}}$, of

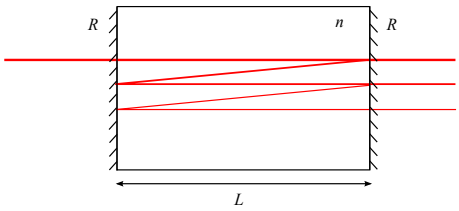


Figure 3.2: *An illustration of how a Fabry-Pérot-interferometer works. The light is transmitted and reflected at each surface (here the reflected beams are drawn beside the original ones, to better illustrate the effect). Multiple interference gives strong transmission for some wavelengths and weak for some.*

the etalon and is calculated according to equation (3.1), where $c$ is the speed of light and $n$ is the refractive index of the material in the etalon.

$$\Delta\nu_{\mathrm{FSR}} = \frac{c}{2nL} \tag{3.1}$$

The transmission of light during one sweep of a diode laser frequency may look something like Figure 3.3. The frequency sweep of the laser can be calibrated by using the free spectral range of the Fabry-Pérot interferometer.

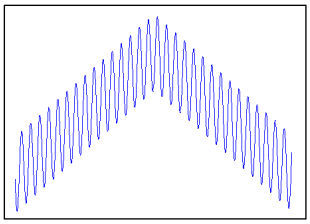

Figure 3.3: *The light from a diode laser transmitted through a Fabry-Pérot etalon when the driving current to the laser is swept up and down.*

The Fabry-Pérot interferometer is useful for frequency-calibration of tunable lasers, but interference fringes can also cause problems in TDLAS, which will be described in the following section.

## 3.3 Optical interference fringe reduction

Reflections from different surfaces of optical components in the light path is often a problem in TDLAS. This is because multiple reflections (between for example the laser and a collimating lens) can cause interference fringes the same way as a Fabry-Pérot etalon does. This can make it hard to detect very weak absorption signals. Optical components like lenses, for example, can be anti-reflex-coated. Fringes that originate from components that cannot be anti-reflex-coated are harder to get rid of.

If the fringes are stable and periodic, they can be subtracted by recording a signal without absorption. The fringes become a problem when they change slowly with time, so that they cannot be treated as a stable background and subtracted from the signal. Especially if the fringes are of the same width and

magnitude as the absorption signal, it will be really hard to distinguish between the absorption signal and the interference fringes.

Optical fringes are especially troublesome in the case that is described in the next chapter, when the gas to be studied is confined inside scattering media. In this case, the scattering samples themselves will give rise to complex interference fringes that cannot be subtracted with the background. One way of reducing the effect of these fringes while measuring on scattering samples is to introduce some "mechanical dithering" in the path, so that the light hits the sample at different places in time. In this work the laser light has been dithered by "tracking coils" (a vibrating lens, taken from CD players). Since the place where the light enters the scattering sample changes all the time, the interference fringes from the samples will also change with time. This turns the effect of the interference fringes into a random signal, which can be reduced by taking an average of many measurements.

## 3.4 Diode lasers

Diode lasers are very suitable for absorption spectroscopy because it is easy to get a stable wavelength tuning. They are made of semiconductor materials with a direct band gap, because these can emit light if a driving current is passed through them (light emitting diodes). Diode lasers are mostly fabricated from doped materials in Group III or V in the periodic table. The structure of diode lasers are explained in detail in [21], and only the basic principles will be given here.

A p-n junction consists of two doped semiconductors, one n-doped and the other p-doped, that are put in close contact with each other. The band gap structure of a p-n junction is shown in the left part of Figure 3.4. The Fermi levels of the two doped materials lie at the same level. If a forward voltage is applied over the p-n junction, a potential difference is established between the Fermi levels of the p-and-n side, which is shown in the right part of Figure 3.4. In this case, there will be population inversion in the so-called depletion region between the p-and-n side, with electrons in the conduction band and holes in the valence band. This means it is possible to get stimulated emission in this region.

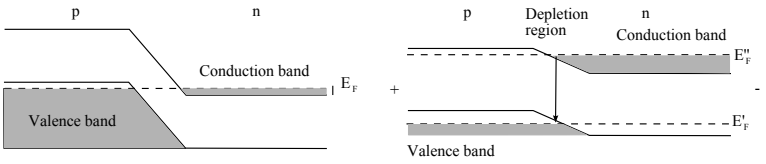


Figure 3.4: *Left: The energy level diagram of a p-n junction. The Fermi energy is at the same level for the p and n side. Right: The energy level diagram of a forward-biased p-n junction. Population inversion is achieved in the depletion region between the p and n side, and thus makes stimulated emission possible.*

This is a simple example of a diode laser. Normally, the structure of the diode laser is more complicated than a simple p-n junction. It may be formed by a double-heterostructure, since these give higher gain than a normal p-n junction.

It is also possible to construct the laser with a quantum-well or quantum-dot structure [21].

This was a description of how population inversion is achieved in a diode laser. A laser cavity is also needed to get laser activity. The cavity can be constructed in different ways, and different structures of the cavity give different names for the laser. Descriptions of three different types of diode lasers are given below.

### 3.4.1 Fabry-Pérot laser

The simplest type of diode laser is called a Fabry-Pérot laser (FP). In this type of laser, the resonator is formed from the surfaces of the laser medium, as is shown in Figure 3.5, where there is high reflectance (30-40%) due to a large difference in the refractive index in the diode and in the surrounding air. The FP laser can have quite high output powers and exists in many regions. A problem with these types of lasers is that there are discontinuous steps in the tuning range of the laser, called mode-jumps. This makes it difficult to use them in TDLAS, since it is hard to make sure that the laser can actually produce the wavelength of the transition in the molecules studied.

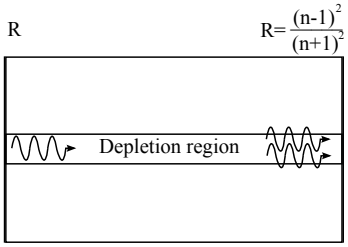


Figure 3.5: *Schematic of a FP laser. The resonator is formed by the surfaces high reflectivity of the surfaces of the semiconductor material.*

### 3.4.2 Distributed-feedback laser

A Bragg grating consists of a material with a periodic variation in its refractive index. This grating will reflect light which fulfills the condition in equation (3.2) below, where $\Lambda$ is the period of the variation in the refractive index, $\lambda$ is the wavelength of the light and $m$ is a positive integer. Because of multiple interference between waves reflected in different layers of the grating, the selectivity of the Bragg grating is high [21].

$$\Lambda = m\lambda/2 \tag{3.2}$$

In a distributed-feedback laser (DFB), a Bragg grating is placed on one side of the depletion region and used to confine light to the depletion region. Since the Bragg grating has a high selectivity in which wavelengths are reflected, the linewidth of the laser becomes narrow [22]. Compared with the FP-laser, the DFB-laser has better tuning abilities and more narrow linewidths but are more costly.

### 3.4.3 Vertical cavity surface emitting laser

A vertical cavity surface emitting laser (VCSEL) works in a similar way as the DFB, with a Bragg reflector both above and below the depletion region. What is special with a VCSEL is that the cavity is perpendicular to the depletion region, instead of parallel to it as in a FP or a DFB laser, allowing an easier fabrication process.

Since the active layer of the VCSEL is thin, the light must pass many times through the active layer and get amplified many times to get laser activity. This means that the Bragg reflector must have high reflectivity, i.e. many layers of alternating refractive index. The output power of a VCSEL is lower than in a DFB, and the threshold current to reach laser action is also lower. The advantages of the VCSEL is that it is easier to manufacture than a DFB and therefore can be purchased at lower cost. It is also normally possible to tune a VCSEL over a larger wavelength span.

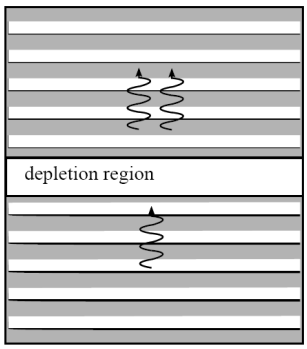


Figure 3.6: *Schematic of a VCSEL. The light passes perpendicular to the depletion region. Bragg reflectors above and below the depletion region act as high reflectivity mirrors.*

# Chapter 4

# Gas in scattering media absorption spectroscopy

A special type of TDLAS is the method to study gas inside strongly scattering solids or liquids. This method is called GASMAS, which is an abbreviation of "GAs in Scattering Media Absorption Spectroscopy". The method was introduced by Sjöholm *et al.* in 2001 [1]. The special features of gas sensing with GASMAS is that the light is heavily scattered when passing through the samples, resulting in long effective path lengths and diffuse light emission from the sample. This chapter goes through the principles of GASMAS. After that, the special case of GASMAS in nanoporous materials will be discussed.

## 4.1 Principles of GASMAS

The basic principle of GASMAS is the difference in the absorption spectra of gases and solids/liquids. Solids and liquids have broad absorption spectra, since the molecules sit closely together and form energy bands, which give absorption lines that are around 10 nm broad. Gases, on the other hand, have sharp energy levels and thus very sharp spectral lines by comparison, typically around 0.001 nm. This means that if free gas is confined in a bulk material (solid or liquid), the absorption of the bulk material will be constant over the short wavelength span of the absorption line of the gas. Therefore, the absorption of the gas can be measured, even when strong scattering causes the light to emerge diffusively out of the scattering bulk material, with weak intensities; see Figure 4.1.

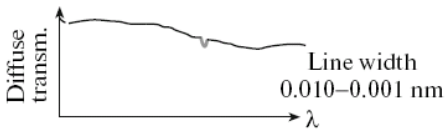


Figure 4.1: *Illustration of the difference between absorption lines in gas and in solids/liquids. The absorption lines of gases are around* $10^4$ *times smaller than the absorption lines in solids/liquids [8].*

In materials with strong scattering, the effective path length of the light

through the gas in the sample is long, in some materials several times longer than the geometry of the sample. This gives a relatively strong absorption of the light passing through the sample.

One very important aspect to take into account when monitoring gas in scattering materials is that the bulk material must not absorb too much at that specific wavelength. This means that it is impossible to measure on absorption lines above 1.4 $\mu$m in materials that contain liquid water, for example human tissue, since the liquid water will then absorb almost all of the light injected into the sample.

In conventional TDLAS, i.e., where free gas is measured either through or in an open air path, the light passes through a gas cell and the transmitted light is measured. Because of the strong scattering in GASMAS measurements, the light will emerge from the sample in multiple directions, making it equally possible to measure in backscattered light as in transmitted, see Figure 4.2.

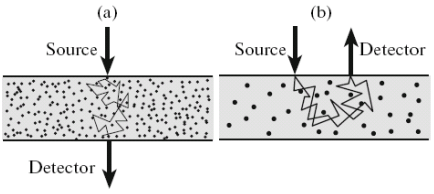


Figure 4.2: *Comparison between the setup for transmission measurements (left) and backscattering measurements (right) [8].*

### 4.1.1 Equivalent mean path length

When measuring the absorption of a gas with TDLAS, the Beer-Lambert law is used to analyze the signal. The problem with this method when performing GASMAS measurements is that the light is scattered inside the material several times, so that the effective path length through gas is unknown. Thus, it is possible to determine the product $NL$ in (4.1), where $N$ is the concentration of the gas in the material and $L$ is the path length through gas in the material, but not each of them individually.

$$I = I_0 e^{-\sigma(\nu)NL} \tag{4.1}$$

A way around this problem is to define an "equivalent mean path length", $L_{\text{eq}}$ through the sample. It is the distance in air, or in some other reference gas, that would give an equally strong absorption signal as the absorption of the gas in the porous sample [23]. The equivalent path length depends both on the concentration of gas in the scattering medium and on the path the light has traveled through the medium. It is given by equation (4.2), where $N_{\text{air}}$ is the concentration of the gas in air, $N_{\text{sample}}$ is the concentration of the gas in the sample, and $L_{\text{sample}}$ is the distance the light has traveled in the sample. In strongly scattering samples, $L_{\text{eq}}$ can be several times larger than the thickness of the sample.

$$N_{\text{air}} L_{\text{eq}} = N_{\text{sample}} L_{\text{sample}} \tag{4.2}$$

If the concentration of the gas in the scattering sample is the same as in the reference gas, the equivalent path length is the mean path length that the light has traveled through the gas. It should be noted that this is not equal to the path traveled through the sample, as the light will travel some distance in the bulk material as well. If the absorption is small, the absorption signal depends linearly on the path length, according to (4.3). $L_{\mathrm{eq}}$ can be calculated by using the standard addition method.

$$I_{\mathrm{t}} = I_0 e^{-\sigma(\nu)NL} \approx I_0 \left(1 - \sigma(\nu)NL\right) \tag{4.3}$$

## 4.2 Gas sensing in ceramics

There are many types of scattering media where GASMAS can be performed. Porous materials are defined as materials that contain small pores of gas in their structure. Examples of porous materials are sintered ceramic powders, like $Al_2O_3$ and $ZrO_2$. They are manufactured by heating ceramic powder and pressing it together. Depending on the conditions for manufacturing, like heat, pressure, particle size and time for manufacturing, they can be made with different pore size distributions. These types of sintered ceramics typically have very strong scattering. The scattering properties of ceramics have been studied in [24].

Typical for GASMAS in ceramics is the strong scattering, which gives long effective path lengths and therefore relatively strong absorption, allowing the absorption signal to be detected directly, without the use of modulation techniques. This makes the line shape analysis of the signals simpler and more straightforward. The diffusion of $O_2$ in most ceramics is very fast [13], so that the pressure inside the pores can be assumed to be the same as in the ambient air, which makes it easier to study absorption at reduced pressures.

## 4.3 Gas sensing in nanoporous materials

As was mentioned in the previous section, sintered ceramics can be manufactured with different pore size distributions. An especially interesting case is when the pores become so small that the mean free path of the molecules become comparable to the size of the pores. In these conditions, the wall collision broadening described in the previous chapter will become a source of broadening comparable with the pressure and Doppler broadening.

GASMAS in nanoporous materials has been studied by Svensson *et al.* in [12] and in [13]. In [12], the absorption of $O_2$ in two different nanoporous alumina ($Al_2O_3$) samples was studied. One sample had a pore size distribution of 70±10 nm, the other 18±2 nm. In the sample with the larger pores, the half width at half maximum (HWHM) of the absorption line was found to be 2.31 GHz, which is a distinct broadening compared with 1.59 GHz for free $O_2$ at the same temperature and pressure. For the sample with the smaller pores, the signal was detected using WMS since the absorption signal was much weaker. Strong line broadening was detected in this sample as well. Furthermore, fitting a Lorentzian curve gave a different HWHM for the first and second harmonics in the WMS signal. The Lorentzian curve also followed the measured absorption

curve badly. This shows that a Lorentzian curve is not a good description for a wall-collision broadened absorption line.

In [13], the absorption of $H_2O$ was studied in the alumina sample with 70 nm large pores. For the strongest absorption line, around 935 nm, the linewidth of the absorption of gas inside the sample was 4.3 GHz, which is a significant broadening compared with 2.9 GHz for free $H_2O$ at the same temperature and pressure. Comparing the two measurements, the broadening due to wall-collisions seems to be stronger for $H_2O$ than for $O_2$, but further studies are needed to establish this.

When the molecules collide with the walls of the pores, they experience a very strong electric field from the electrons in the wall. This case is very similar to the Stark effect, where an external electric field causes a shift of the energy levels of the molecules. Thus, a shift of the absorption lines might be expected when molecules are confined in nanoporous materials. Such a shift has been observed in [25], where water vapour absorption has been studied in nanoporous silica aerogel.

The interaction between molecules and walls is a very interesting physical effect, and the gas sensing in nanoporous materials gives a unique opportunity to actually study the effects of the wall collision broadening. Studying the absorption lines may also in the future have applications in structure analysis of nanoporous materials, such as non-intrusive measurement of the pore size, porosity etc.

# Chapter 5

# Instrumentation

In this chapter the instrumentation used for the measurements will be discussed. In the first section, the instrumentation used for the GASMAS measurements are described. Next, the pressure chamber and the gas control systems are more closely examined. After that, there is a section where the performance of the molecular oxygen system is characterized with Allan deviation. Finally, there is a description on the automatic process to determine the optimal number of averages for the $O_2$ system.

## 5.1 GASMAS setup

Here, the setups for the GASMAS measurements will be described. There are three different setups, each to be used for measuring GASMAS on either molecular oxygen, water vapour or carbon dioxide.

### 5.1.1 $O_2$ - Molecular oxygen

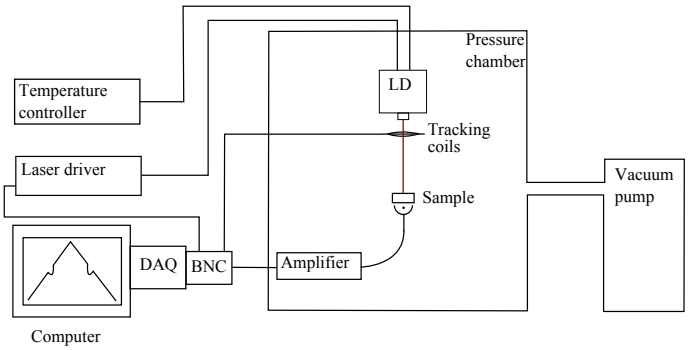


Figure 5.1: *The GASMAS instrumentation for measuring on $O_2$ at 760 nm.*

The setup used for measurements on molecular oxygen in the A-band is shown in Figure 5.2. A single-mode VCSEL, from Laser Components, emitting at 760 nm is used. The laser is controlled by a laser driver LDC200V and a temperature controller TED200C from Thorlabs. The light is sent from the

laser diode through the tracking coil onto the sample of scattering medium, which is normally a sample of some ceramic, but can also be something else.

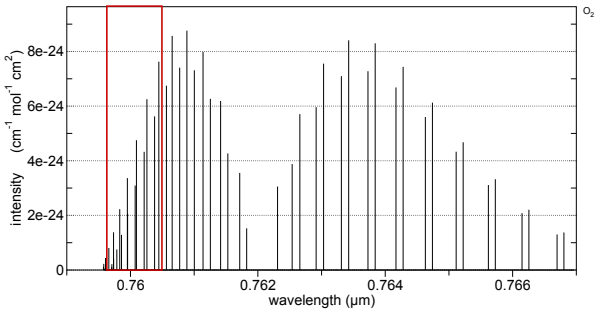


Figure 5.2: *The absorption spectrum of $O_2$ in the tuning range of the laser [17]. The lines belong to the oxygen A-band. The lines within the red rectangle are within the tuning range of the laser.*

The sample is placed on top of a $5.6 \times 5.6$mm photodiode, which detects the diffuse light emerging from the sample. The signal from the detector is then sent through a current amplifier of type DLPCA - 200 from FEMTO, and connected through a BNC board (BNC2110, National Instruments), to the DAQ card (NI, PCI-6132) into the computer. In the computer, the signal is analyzed with a program in LabView.

It is better to study the effect of the wall-collision broadening at lower pressures, since the effect of the pressure broadening decreases with the pressure. Therefore, the laser, sample and detector are placed in a pressure chamber, which is more closely explained in the section on the gas control system. This chamber can be pumped down to pressures of around 1 Torr. To increase the magnitude of the signal, it is possible to flush the pressure chamber with pure $O_2$.

### 5.1.2 $H_2O$ - Water vapour

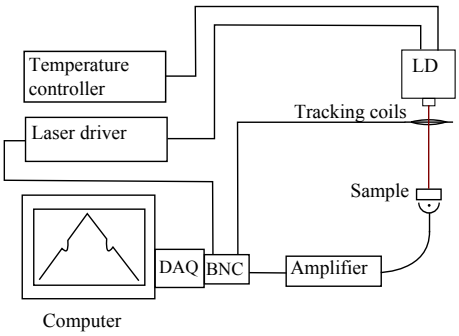


Figure 5.3: *The GASMAS instrumentation for measuring on $H_2O$ at 948 nm.*

The setup that was built to measure on water vapour around 948 nm will now

be described. The spectrum for $H_2O$ in this wavelength region is pictured in Figure 5.4. The laser source is a single-mode VCSEL, from Laser Components. It is controlled by a laser driver LDC200V and a temperature controller TED200 from Thorlabs. The light is sent through a tracking coil onto the sample, which is placed on top of the $5.6 \times 5.6$mm photodiode. The signal from the detector is sent through a DLPCA 200 current amplifier from FEMTO, which then passes through a BNC board (BNC210, National Instruments) to a DAQ card (NI, PCI-6120). The DAQ card digitalizes the signal, which is then analyzed in a LabView program in a computer. The LabView program also controls the modulation of the driving current through the laser.

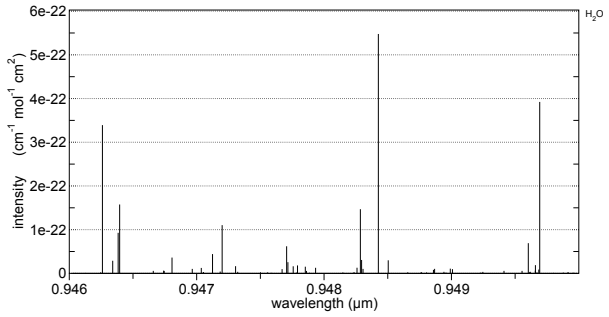


Figure 5.4: *The spectrum of water vapour at 948 nm [17].*

Unfortunately, the VCSEL broke after the setup was finished. Should a new laser be purchased, it would probably be possible to use this setup and measure on $H_2O$ in nanoporous materials.

### 5.1.3 $CO_2$ - Carbon dioxide

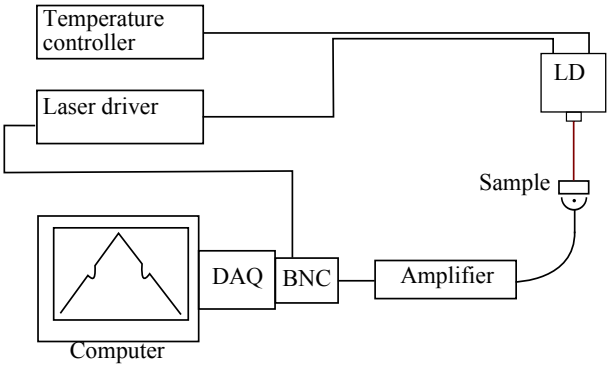


Figure 5.5: *The GASMAS instrumentation for measuring on $CO_2$ at 2.055 $\mu$m.*

The laser used for measuring on $CO_2$ is a DFB laser from Toptica Photonics operating at 2.055 $\mu$m. The spectrum around this wavelength is shown in Figure 5.6. The laser is controlled by a LDC201CU laser driver and a TED200C

temperature controller, both from Thorlabs. The detector is a 1x3 mm large PbSe photoconductive detector.

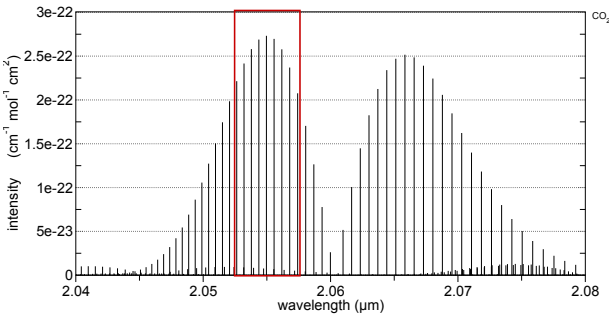


Figure 5.6: *The spectrum of carbon dioxide at 2.055 μm [17]. The lines inside the red rectangle are within the tuning range of the laser.*

The current from the laser driver to the laser diode is modulated with a triangular wave by a signal from the computer. The signal from the photodiode is collected via a BNC block (BNC210, National Instruments) to the DAQ card (NI, PCI-6120) and into the computer, where it is analyzed with a program in LabView.

## 5.2 Gas control system

As has been mentioned in previous chapters, it is easier to see the wall collision broadening if the GASMAS measurements are performed at low pressures. To achieve this, a pressure chamber has been built, which can be pumped down to low pressures, around 1 Torr, even if it cannot achieve complete vacuum.

A problem when measuring at really low pressures is that, although the pressure broadening becomes less pronounced, the absorption signal also decreases. One way to increase the absorption signal while still measuring at low pressures is to increase the concentration of $O_2$ in the gas. To achieve this, a gas tube containing pure $O_2$ was purchased and the pressure chamber was modified with a gas inlet, as can be seen in Figure 5.7. The gas inlet was tested with $N_2$, to check that there was no leakage.

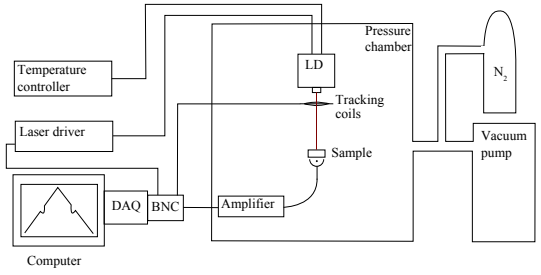


Figure 5.7: *Schematic of the setup used for the measurements. The $N_2$ is flowed into the gas chamber via the vacuum pump inlet.*

The measurements were performed on a zirconia ceramic with heavy scattering. The absorption of light by $O_2$ inside the sample at an air pressure of 100 Torr is shown in Figure 5.8.

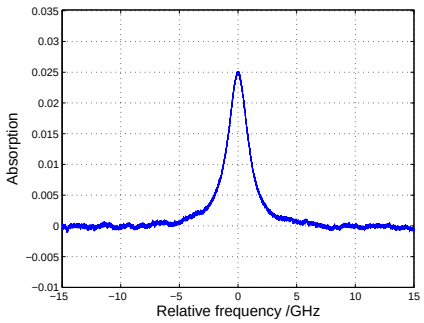


Figure 5.8: *The absorption of $O_2$ in zirconia at 100 Torr pressure in air*

Now the pressure in the chamber was first lowered to around 4 Torr and then filled with $N_2$ to a pressure of about 100 Torr. The absorption signal of $O_2$ after this is shown in Figure 5.9. It can be noted that there is still an absorption signal of $O_2$ in the sample. If the system had worked perfectly, there would not have been any absorption signal since the chamber would have been filled with pure $N_2$. However, there is still a small signal, even if it is much smaller than the signal in air. It has been checked before that the sample has open pores and that the diffusion of $N_2$ and air is very fast, so gas lingering in closed pores should not be a problem.

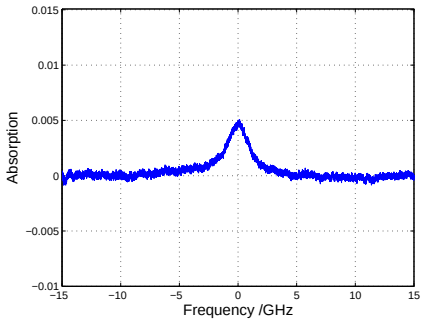


Figure 5.9: *The absorption of $O_2$ in zirconia with the pressure chamber filled with $N_2$ at 100 Torr*

Now more $N_2$ was flushed into the chamber until the pressure was 200 Torr. The resulting absorption of $O_2$ is shown in Figure 5.10. The signal seems to have decreased when the pressure of $N_2$ was raised, if figures 5.9 and 5.10 are compared, although the difference is very small. It may be that the absorption signal of $O_2$ comes from a small amount of $O_2$ that did not get out of the chamber as it was emptied. That seems reasonable, since the chamber was not pumped down to full vacuum before $N_2$ was let into the chamber. The result

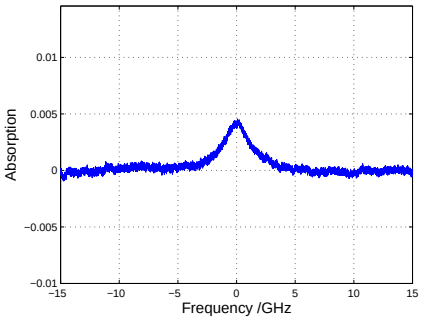


Figure 5.10: *The absorption of $O_2$ in zirconia with the pressure chamber filled with $N_2$ at 200 Torr*

might get better if the chamber is repeatedly flushed with $N_2$, emptied and then flushed again.

Even if there is a small amount of air still left in the chamber after flushing the chamber with $N_2$, it might not be a big problem. The goal with the gas control system was to enhance the absorption signal by measuring on a higher concentration of $O_2$. Since the exact concentration of $O_2$ is not interesting, it should not be a problem if the measurements were performed on 95 % $O_2$ instead of 100 %. The only real problem would be if there was a leakage of pure $O_2$ out of the chamber, which there does not seem to be.

## 5.3 Characterization of system performance

To characterize the performance of a system, there is a method called Allan deviation analysis. It was originally developed to measure frequency stability in clocks, but it can also be used to characterize the performance of other types of measurement systems. The Allan deviation analysis can help determine the number of averages that optimize a measurement signal. This section will start by describing the basic principles of Allan deviation analysis. After that, the result from the Allan deviation measurements on the $O_2$ system will be presented.

### 5.3.1 Principles of Allan deviation analysis

Allan deviation analysis starts by measuring some quantity, for example the peak absorption of oxygen in a porous ceramic. To start with, take one measurement point each second. This gives a number of peak absorptions that vary around a certain mean value. The next step is to form an average of two successive measurements. Then, the average of three successive measurements will be taken. The result will be something like Figure 5.11.

The $k$th average represent the signal after an average time of $k$ seconds. It can be seen in Figure 5.11 that the signal gets less spread out from the mean value the longer the averaging time. This means that the standard deviation is reduced. Now, the principle is to take the standard deviation of all these averaged measurements, from average time 1 second up to average time $n$ seconds.

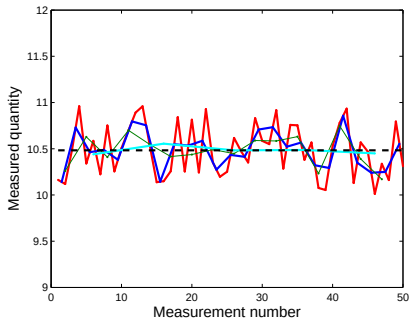


Figure 5.11: *This figure illustrates the principle of Allan deviation analysis. The red curve follows 100 random numbers centered around 10.5. The dark blue curve shows the curve after an average has been made out of two adjacent points. In the green curve, the average is between 3 adjacent points, the turquoise with four adjacent points, and so on. It can be noted that the standard deviation of the values decreases with increasing averaging time.*

This gives the Allan deviation as a function of the averaging time.

An example of how an Allan deviation plot of a system may look like is shown in Figure 5.12. The Allan deviation normally decreases as the averaging time increases up to a certain point, as the random noise is averaged away. After a certain amount of time, the deviation will starts to increase, since drifts in the system can limit the averaging process.

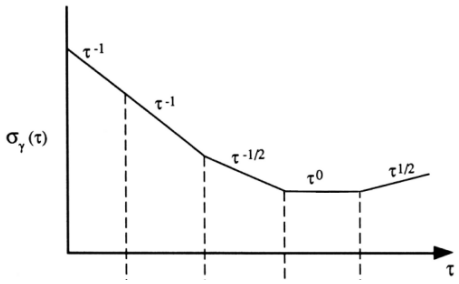


Figure 5.12: *A simple example of how an Allan deviation plot may look [26].*

### 5.3.2 Allan deviation on the $O_2$ system

To characterize the system performance of the system for measuring $O_2$, the absorption was measured with an averaging time of 1 second (i.e. 18 averages) for approximately 2 hours. The peak absorption and the half width at half maximum (HWHM) was calculated for each of these measurements. The calculated values are represented in Figure 5.13.

Figure 5.14 show the Allan deviation for the peak absorption and the HWHM for these measurements. It can be noted that the Allan deviation has not started to go up again, but that it has started to flatten out to a constant value.

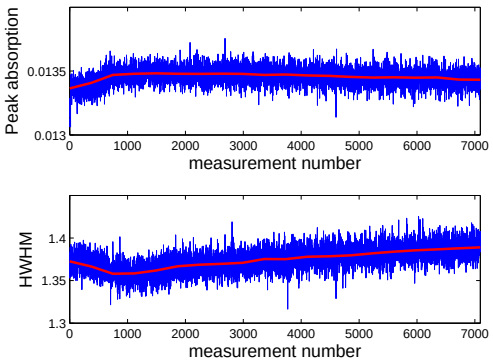


Figure 5.13: *Top: The peak absorption during the measurements. The red curve shows the absorption calculated with an averaging time of 354 s. Bottom: The HWHM during the measurements. The red curve shows the HWHM calculated with an averaging time of 354 s.*

It can be noted that the decrease in the Allan deviation seems to have stopped around averaging time of 200 seconds. If the measurements had continued for a longer time, it would probably have started to rise upwards again. These Allan deviation results seem to indicate that it is not worth the trouble to measure with averages longer than around 3 1/2 minutes.

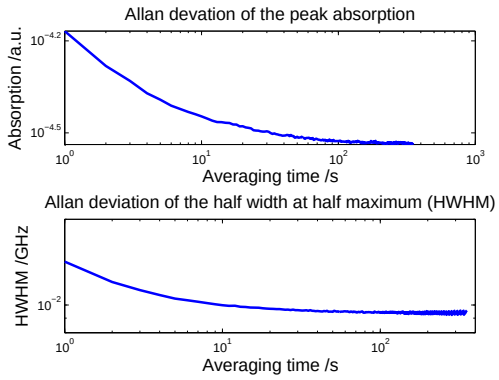


Figure 5.14: *The Allan deviation for the peak absorption (top) and the HWHM (bottom) as a function of the averaging time.*

## 5.4 Averaging system

The GASMAS instrumentation collects the data by taking an average of a number of measurements, in order to get a good result and to get rid of random noise. As we saw in the previous section, it is not easy to determine the number of averages that will give the best result. A higher number of averages gives a better result up to a certain point, after which it seems to be pointless to take

more averages. Choosing the averaging time may be tricky, since the optimal time can vary from sample to sample, or with different conditions in the measurement system. A longer averaging time also means a lot of waiting while the measurements are taken. A LabView program for the $O_2$-system that will automatically stop the averaging process when the signal seems to have stopped improving has been developed as part of this Master's project. This could both save time and give better measurements.

In this section the principles of the automatic averaging program will be presented, along with measurements on polystyrene foam to check how well the program works for GASMAS measurements.

### 5.4.1 The standard deviation of the change in the averaging process

The automatic determination of the optimal number of averages will be determined by measuring the change in the standard deviation of the difference between two successive averages. We will call the signal averaged after $n$ measurements $\bar{A}$, and it is calculated according to equation (5.1).

$$\Delta A = |\bar{A}_n - \bar{A}_{n+1}| \tag{5.1}$$

The next step is to take the standard deviation of the difference in the averaged measurements. We call the standard deviation after $n$ measurements $\sigma_n$. Figure 5.15 shows how the standard deviation of the measurements changes during 1080 measurements. The idea of the automatic averaging process is to stop the averaging process when the standard deviation is lower than a certain tolerance.

S 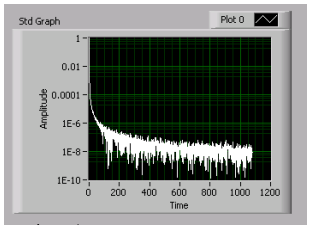


Figure 5.15: *The standard deviation for the averaging of the measurements on $O_2$ in polystyrene foam.*

It can be noted that there are "spikes" in an otherwise smooth curve of the standard deviation. This probably happens when the difference between two successive averages happen to vary very little. We want to stop the averaging process when the smooth curve reaches beneath the tolerance, not when one of these "spikes" happens to go below it. To achieve this we take instead the average of 10 successive standard deviations and check when this reaches below the tolerance. We call the average of the standard deviation after n averaged measurements $\bar{\sigma_n}$. The average was computed according to equation (5.2).

$$\bar{\sigma_n} = \frac{1}{10} \sum_{n}^{n+10} \sigma_n \tag{5.2}$$

Figure 5.16 shows how $\bar{\sigma_n}$ changed during 5400 averages. It can be noted that the standard deviation decreases slowly after it has gone below $10^{-8}$. Thus a suitable stopping criteria may be around this value.

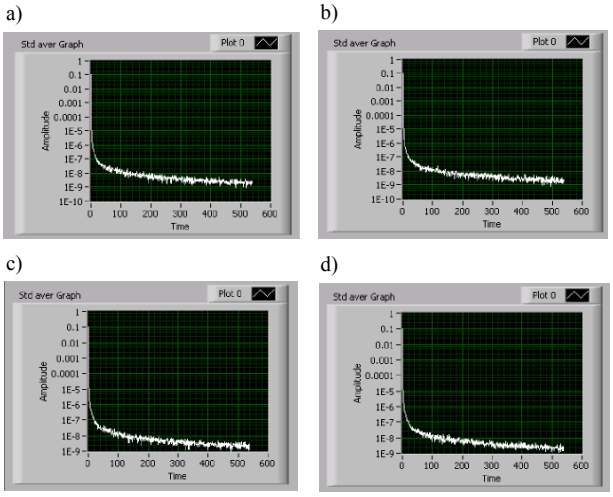


Figure 5.16: *The change in the average standard deviation for the averaging of absorption measurements on $O_2$ in polystyrene foam during 5400 averages. Figures a)-d) show four successive measurements. The "time" on the x-axis shows the number of averages divided by 10.*

### 5.4.2 Number of averages for different tolerance

The tricky part with this averaging process is to set the tolerance so that the averaging process does not stop too early, which would give more noisy measurements. With Figure 5.16 in mind, the tolerance should be somewhere between $10^{-7}$ and $10^{-8}$. To test which value that was best, the absorption in polystyrene foam was measured for different tolerance, and the number of averages required to reach that tolerance was noted. Figure 5.17 shows the number of averages that were needed to reach each tolerance. Table 5.1 shows the mean value and the median value needed to reach a certain tolerance, and the standard deviation of the number of averages for each tolerance.

Table 5.1: *The mean, median and standard deviation of the number of averages needed to reach a certain tolerance in the standard deviation of the change in the averaging process.*

| Tolerance | | $10^{-7}$ | $5 \cdot 10^{-8}$ | $2 \cdot 10^{-8}$ | $10^{-8}$ |
|---|---|---|---|---|---|
| Number of averages: | Mean value | 207 | 288 | 518 | 837 |
| | Median value | 205 | 290 | 520 | 825 |
| | Standard deviation | 9.7 | 19 | 42 | 100 |

The number of averages needed to reach a certain tolerance will of course vary depending on the samples that are measured on, and other conditions. However, from these measurements it looks as if $10^{-8}$ is a suitable tolerance.

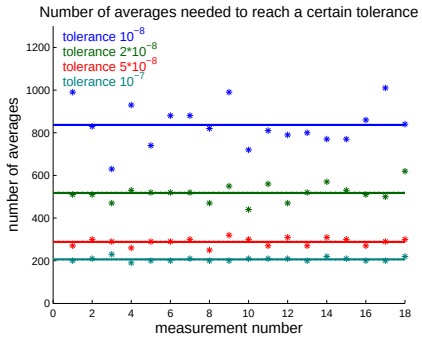


Figure 5.17: *The number of averages needed to reach a certain tolerance in the averaging process. The stars show the value obtained in each separate measurement and the lines show the mean number of averages for each tolerance.*

# Chapter 6

# Pressure dependence investigation of the setup

In this chapter, the behavior of the system for GASMAS measurements on $O_2$ at lower pressures is investigated. First, the absorption of $O_2$ in polystyrene foam was measured. Then, the diffusion in polystyrene foam was investigated. Finally, the absorption of $O_2$ in macroporous alumina is measured at low pressures.

## 6.1 Polystyrene foam

At lower pressures, the wall-collision broadening of the absorption lines should become more visible since the pressure broadening decreases. To check that there is no additional line-broadening mechanism at low pressures, the absorption of light by $O_2$ in polystyrene foam, which does not have nanometer-sized pores, was measured at low pressures; see Figure 6.1. If these measurements have the broadening and line shape predicted by Doppler-and pressure broadening, then the additional line-broadening in nanoporous materials can be assumed to arise from the wall-collision broadening and nothing else.

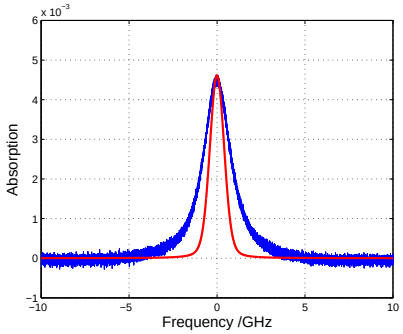


Figure 6.1: *Absorption in polystyrene foam at 50 Torr (blue curve), compared with the Voigt-profile for absorption at 50 Torr (red curve).*

It can be noted that the absorption lines are much broader than the theoretical line width of absorption at that pressure. A plausible reason for this result is that the diffusion of gas out of polystyrene foam is slow, which was noted in [1] and [27]. This will be examined in the following section

## 6.2 Diffusion of $N_2$ in polystyrene foam

One explanation for the broad absorption lines in polystyrene foam at low pressures could be that the diffusion of gas out of the sample is slow. Then the gas in the pores of the sample would have a different pressure than the ambient air in the pressure chamber, and the line shapes of the measured samples would correspond to this pressure instead of the pressure in the chamber. To check if this was the case, a sample of polystyrene foam was flushed with $N_2$. The absorption of $O_2$ was measured shortly after the flushing started, and the result is shown in Figure 6.2.

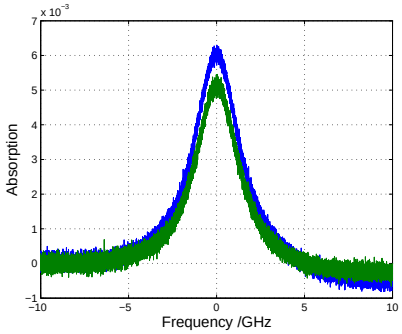


Figure 6.2: *Absorption of oxygen in polystyrene foam. The blue curve shows the signal when the sample was in open air and the green curve shows the signal when the sample was flushed with $N_2$.*

Since the absorption signal does not disappear immediately when the sample is flushed with $N_2$, the gas diffusion out of this sample of polystyrene foam seems to be slow. This is in agreement with results in [1] and [27]. The diffusion of $O_2$ at low pressures in polystyrene foam will be examined next.

## 6.3 Diffusion at low pressures in polystyrene foam

Diffusion processes can normally be described by Fick's second law of diffusion,

$$\frac{\partial C}{\partial t} = D\frac{\partial^2 C}{\partial z^2}, \tag{6.1}$$

where $D$ is the diffusion coefficient, $C$ is the gas concentration, $t$ is the time and $z$ is the spatial coordinate along which the diffusion process takes place. The solution to this equation for the GASMAS case is a rather complicated mathematical formula [27].

In the later part of the diffusion process, the solution can be approximated by an exponential curve with a well-defined time constant. This means that the peak absorption can be described by equation (6.2). If this is the case, the logarithm of the absorption should follow a straight line, see (6.3).

$$A = a \cdot e^{-t/\tau} + d \tag{6.2}$$

$$\ln(A - d) = -t/\tau + \ln a \tag{6.3}$$

Here $A$ is the peak absorption of $O_2$, $t$ is the time after the diffusion started, $\tau$ is the time constant of the diffusion process, $a$ is a constant and $d$ is the peak absorption when the diffusion has stopped, i.e. when the pressure is the same inside the pores as in the chamber.

To see if the diffusion of gas out of polystyrene foam at low pressures can be described like this, the sample of polystyrene foam was placed inside the the pressure chamber and the pressure was lowered to 50 Torr. After this, the absorption in the sample was measured every minute for an hour. The peak absorption for each of the measurements is shown in Figure 6.3 as a function of the time after the measurements started. An exponential function like equation (6.2) has been fitted to the measurements.

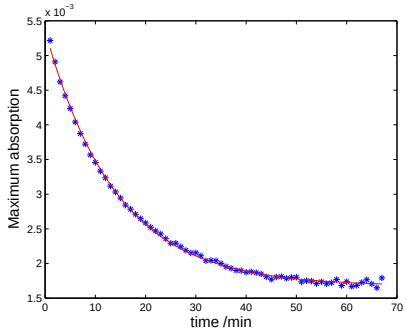


Figure 6.3: *The absorption in polystyrene foam as a function of the time the sample has spent at the pressure 50 Torr*

The exponential function agrees very well with the measured values. The logarithm of the absorption was also plotted; see Figure 6.4. The measured values follow an almost perfect straight line in the beginning of the measurements, as predicted by equation (6.3). This shows that the diffusion process can be described by an exponential equation. After around 40 minutes, the diffusion process seems to have finished, which is why the points no longer follow the straight line.

From these measurements, it seems that the diffusion of gas out of polystyrene foam can be described by an exponential equation. This probably means that when the measurements started, the diffusion process had passed the part of the process that cannot be described by an exponential function.

It should be noted that the absorption in equation (6.2) refers to the total absorption of light, i.e. the area under the absorption line, and not the peak absorption. As the pressure decreases, the line shape of the absorption line changes since the pressure broadening decreases. This means that the peak

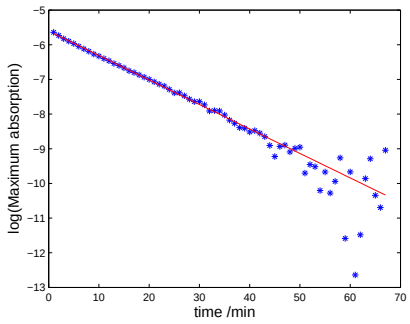


Figure 6.4: *The logarithm of the absorption in polystyrene foam as a function of the time the sample has spent at the pressure 50 Torr*

absorption does not have the same relation to the total absorption at different pressures. A more correct analysis of the diffusion process would be to plot the total absorption as a function of time.

## 6.4 Macroporous alumina

To see whether the system gives the expected line shapes at low pressures, the absorption of $O_2$ at low pressures was measured on a sample of macroporous alumina, $Al_2O_3$; see Figure 6.5. It has been confirmed that the diffusion of $O_2$ in this sample is fast.

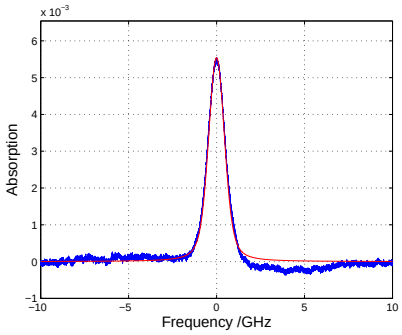


Figure 6.5: *Absorption in macroporous alumina at 100 Torr (blue curve) compared with the theoretical line shape at the same pressure*

The absorption line fits reasonably well with the theoretical line shape of the Voigt profile. The small deviation in the right wing in Figure 6.5 could come from some sort of background noise, or it could arise from a bad baseline fit in the calculation of the absorption. This measurement seems to indicate that the system gives the correct line shapes at low pressures for gas in macroporous materials.

# Chapter 7

# Measurements

This chapter will show the results of the measurements that have been performed in this Master's thesis. The first section will deal with the wall-collision broadening of the absorption lines of $O_2$ in samples of nanoporous zirconia at different pressures. The width of the absorption lines will be compared with the theoretical line shape of a free gas at the same pressure. The line-broadening effect due to wall-collisions will be clearly visible. The measurements have been taken for two ceramic samples with different pore size distribution, and it will be quite clear that the broadening of the absorption lines is larger in the sample with the smaller pore size distribution.

The next section will show the results of the GASMAS measurements on $CO_2$. The measurements have been performed both in straight light paths, in polystyrene foam and in macroporous and nanoporous ceramics.

## 7.1 Absorption of $O_2$ in nanoporous zirconia

In this section the wall-collision broadening of the absorption lines of $O_2$ in nanoporous ceramics is compared to the theoretical line shape of free $O_2$ at the same pressures. It has been verified that the diffusion of $O_2$ out of the zirconia samples is fast, so the pressure inside the pores can be assumed to be the same as in the ambient air.

Figure 7.1 shows the absorption of $O_2$ in nanoporous zirconia the pressures of 50 Torr, 100 Torr and 200 Torr. The blue line shows measurements on a sample with 43 nm pores, the green a sample with 115 nm large pores. The red line shows the theoretical line shape at the same pressures, the Voigt profile. It is calculated by taking the convolution of the theoretical pressure broadening, a Lorentzian curve, and the theoretical Doppler broadening, a Gaussian curve. The half width at half maximum (HWHM) is shown i the figure for each pressure and sample/simulation.

It has been shown in [28] that the HWHM as a function of pressure is a straight line. This trend can be seen in Figure 7.2, where the HWHM has been plotted as a function of pressure for the three pressures in Figure 7.1. Here it can also be clearly seen that the broadening is larger in the sample with the smaller pore size.

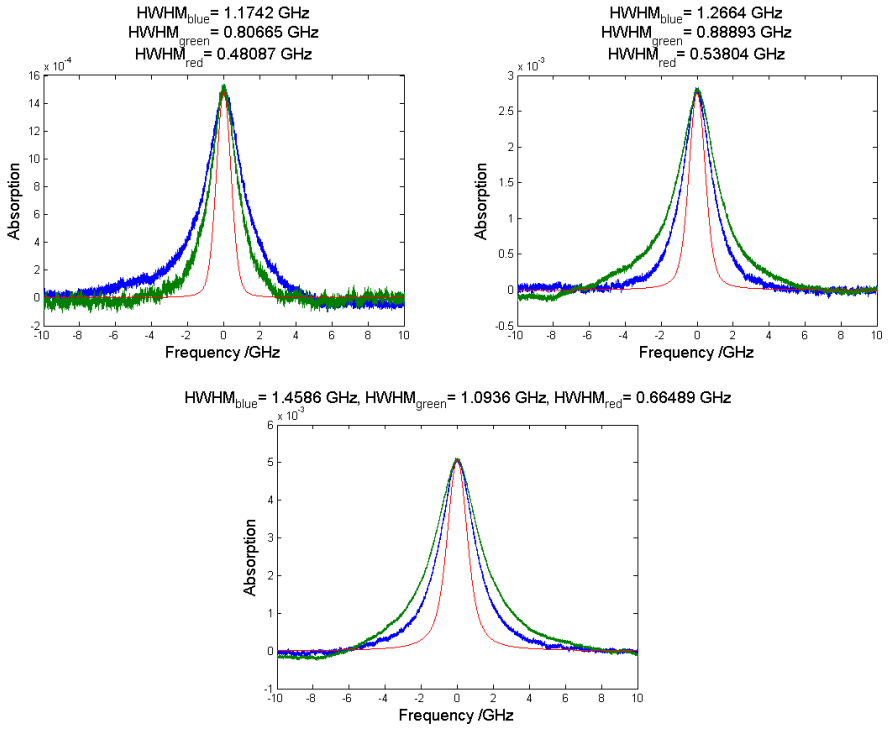


Figure 7.1: *Upper left: The absorption of $O_2$ at 50 Torr. The blue line is the sample with the smaller pore size, the green the larger pore size and the red the Voigt profile. Upper right: The absorption at 100 Torr. Lower: The absorption at 200 Torr. The HWHM are given for each curve.*

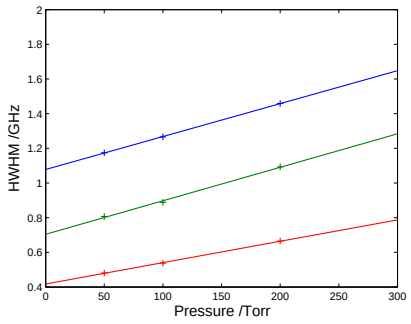


Figure 7.2: *The HWHM as a function of pressure. The blue curve is for the sample with the smaller pore size, the green the sample with the larger pore size and the red the Voigt profile.*

## 7.2 $CO_2$ GASMAS

### 7.2.1 $CO_2$ GASMAS in polystyrene foam

With the setup described in the instrumentation chapter, the absorption of $CO_2$ in a 1 cm thick sample of polystyrene foam has been measured. To increase the concentration of $CO_2$ in the sample, it was placed inside a plastic bag that had been breathed in and out of a few times. As it has been shown that the diffusion of gas in and out of polystyrene foam can be slow, the sample was left in the plastic bag for around 40 minutes.

The absorption of $CO_2$ in a straight path through a plastic bag is shown in Figure 7.3. The absorption of light that has passed through the sample of polystyrene foam is shown in Figure 7.4. The frequency scale on the x-axis has not been calibrated, but existing data show that the line width of the absorption lines of $CO_2$ at this wavelength is around 10 GHz, which means that the frequency scan of the laser in Figures 7.3 and 7.4 is approximately 70 GHz.

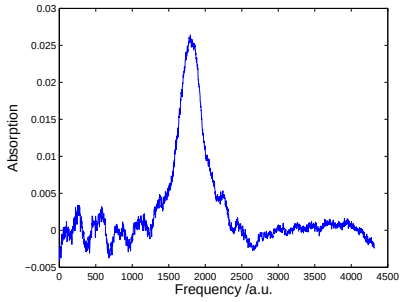


Figure 7.3: *Absorption of $CO_2$ in an approximately 12 cm straight path through a plastic bag with unknown concentration of $CO_2$.*

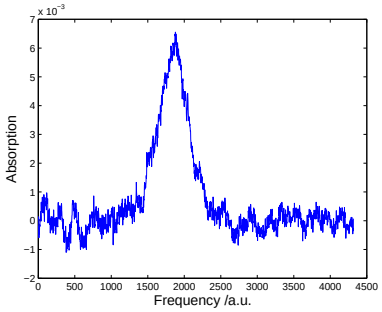


Figure 7.4: *Absorption of $CO_2$ in an approximately 1 cm thick sample of polystyrene foam.*

There is a clear absorption of $CO_2$ both in the straight absorption path and in the sample of polystyrene foam, even if the detected signal is quite noisy. That the signal is weaker in polystyrene foam may be because of a shorter path length through gas or lower concentration of $CO_2$ in the plastic bag, or perhaps a combination of both.

### 7.2.2 $CO_2$ GASMAS in polystyrene foam and ceramics

The setup was also used to measure $CO_2$ inside porous ceramics. Here, the signal was weaker than in polystyrene foam, so the measurements were performed on polystyrene foam as well, and the absorption in the two samples was compared.

Figure 7.5 shows the absorption signal in polystyrene foam and a 2.9 mm thick sample of macroporous alumina, measured with the same settings on the laser driver and temperature controller. The signal in polystyrene foam has been normalized to have the same peak value as the signal in the ceramic sample. Since the absorption in the alumina sample was weaker, the noise is more dominant in that signal than in the signal from polystyrene foam.

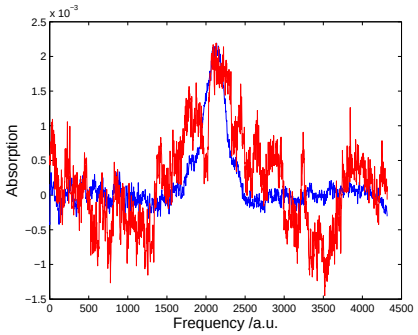


Figure 7.5: *Absorption of $CO_2$ in polystyrene foam (blue) and in macroporous almina (red). The signals have been normalized to have the same peak value.*

Figure 7.6 shows the absorption in polystyrene foam and in nanoporous alumina. The signal in polystyrene foam has been normalized to have the same peak value as the signal in the ceramic sample. The absorption of $CO_2$ in the sample of nanoporous alumina in Figure 7.6 is very weak and therefore hard to separate from the background noise, but since the signal has a peak at the same value as the stronger signal from polystyrene foam, it can be assumed to be an absorption signal.

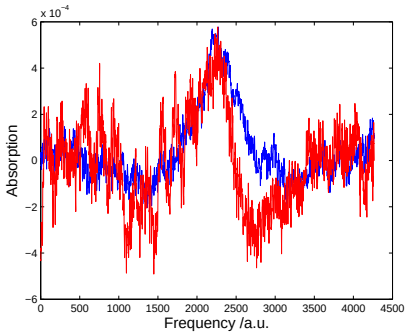


Figure 7.6: *Absorption of $CO_2$ in polystyrene foam (blue) and in alumina with 70 nm large pores (red). The signals have been normalized to have the same peak value.*

# Chapter 8

# Discussion

## 8.1 $O_2$ GASMAS

### 8.1.1 Wall-collision broadening in nanoporous materials

The absorption of light by $O_2$ in nanoporous zirconia ceramics has been measured at low pressures, and the additional line-broadening due to wall-collisions can be clearly seen. The effect is similar to previous measurements in nanoporous materials in [12], [13] and [28].

It has been shown in [11] that the line-broadening due to wall collisions and intermolecular collisions can be treated separately and then added together to give the total line broadening due to collisions. In Figure 7.2, the line width increases linearly with pressure, supporting this theory. There are not enough measurements in this figure to say anything for certain, but more measurements have been performed in [28] to confirm this.

In Figure 7.1, a clear difference between the broadening in the two samples with different pore size distribution can be seen. This indicates that it could be possible, in the future, to use the line-broadening due to wall collision as a non-intrusive method for measuring pore size of nanoporous materials. Right now, it is possible to compare similar nanoporous materials and determine which sample has the smallest pore size.

It is difficult to analyze the line shape of the absorption lines, because the absorption profile is also affected by the pressure and Doppler broadening. More thorough studies are required for this analysis, and to observe the small shifts that were measured in [25].

### 8.1.2 Diffusion in polystyrene foam

It has been verified that the diffusion of gas out of polystyrene foam at low pressures is a relatively slow process. This has also been examined in [1] and [27], where the diffusion of $O_2$ into a sample of polystyrene foam after it had been lying in pure $N_2$ for a long time, was studied.

The diffusion process at low pressures, presented in Figure 6.3, follows an almost perfect exponential curve. This shows enough time has passed when the measurements started that an exponential equation is a good approximative solution to Fick's law. The time constant for the diffusion was determined to

be 14 minutes, but analyzing the peak absorption as a function of time does not describe the diffusion properly, since the line shape of the absorption line changes as the pressure decreases. A study of the total absorption as a function of time would probably give a smaller time constant than the one found here, as the peak absorption becomes larger in relation to the total absorption when the line width decreases. It has also been shown in [27] that the time constant for diffusion in polystyrene foam can be quite different for different samples.

One conclusion that can be drawn from these diffusion measurements is that it is necessary to check if the diffusion of gas is quick or slow before drawing any conclusions about the line width in a nanoporous sample. If the diffusion is slow, too early measurements will show a broader absorption line than expected because of higher pressure inside the sample than in the ambient air.

### 8.1.3 System improvements

The gas inlet system that was built to enable measurements with pure $O_2$ has been successful. It has not yet been tested with $O_2$, but the inlet worked well with $N_2$, and flushing the chamber with $O_2$ should work in the same way. The fact that it is hard to achieve 100% $O_2$ in the chamber is irrelevant, as the exact concentration of $O_2$ is not important. The important thing is that a higher concentration of $O_2$ could allow measurements at even lower pressures, which could help the investigation of the line shape and line width due to wall collisions.

The automatic averaging program also seems to be working as it was intended to work. The problem here is to find a way to determine a suitable tolerance as a stopping criterion. An Allan deviation may be useful for determining the tolerance, but it takes time and the Allan deviation may vary between different samples and with different measurement conditions. The method right now is to test a few times and choosing what looks like a suitable tolerance. Advantages with the automatic averaging program is that it could save time, since the measurements do not go on for a longer time than necessary. It could also lead to better measurement results, since the averaging process will stop before drift noise causes the measurements to get worse.

### 8.1.4 Allan Deviation

The Allan deviation measurements in Figure 5.14 show that the averaging process gives an optimal result for an almost 2 minutes long averaging time. It looks like the detection limit is an absorption of approximately $3 \cdot 10^{-5}$, corresponding to an equivalent path length in air of around 1.5 mm. This result can be compared to the measurements presented in [29], where an Allan deviation showed a detection limit of 0.1 mm. These measurements used WMS, which greatly improve detection sensitivity, so it is not surprising that our measurements have lower sensitivity. The detection limit for the HWHM seems to be around 0.01 GHz.

The Allan deviation probably depends on the measurement conditions. For example, the amplitude of the vibrations of the tracking coils can change the detection limits. The Allan deviation is most likely different depending on the sample that is being measured.

## 8.2 $CO_2$ GASMAS

It has been established that it is possible to measure on $CO_2$ in scattering media. The detector used is not optimal for these type of measurements since it gives relatively much noise, making it hard to see the signals. To improve detection sensitivity, a better detector should be purchased. Another way of increasing detection sensitivity could be to use tracking coils or vibrators to reduce interference noise.

The measurements are unfortunately too noisy for an analysis of the line shape of the signal in the nanoporous material. Measurements at low pressures may also be necessary, to see any clear line broadening due to wall collisions. Before this, it would probably be necessary to check the diffusion properties of $CO_2$ in the samples, since that has been found to be very different when comparing $H_2O$ and $O_2$.

When comparing Figure 7.3, the absorption of $CO_2$ in a 12 cm straight path, to values obtained from [17], the concentration corresponding to that strength of absorption is around 7%. Assuming that the concentration is the same in the sample of polystyrene foam, whose absorption is shown in Figure 7.4, the equivalent path length in the sample of polystyrene foam is around 3 cm, again by comparing with data from [17]. In the same way, the equivalent path length in macroporous alumina would be around 1 cm, for 2.9 mm thick sample, and 3 mm in nanoporous alumina, for a 2 mm thick sample.

This is of course only a rough estimation, as the concentration of $CO_2$ in the plastic bag with the different samples is probably different. As the diffusion of $CO_2$ has not been examined, it could also be that slow diffusion caused lower concentration in the samples than in the rest of the bag, even though every sample was allowed to lie in the bag for at least 25 minutes before measuring. For a more accurate path length, measurements would have to be performed at known concentrations. However, this first estimation indicates a shorter path length, i.e. weaker scattering, for light of this wavelength compared to the wavelength used to measure on $O_2$ [12].

# Chapter 9

# Summary and future work

## 9.1 Summary

The absorption of light by $O_2$ confined in nanoporous zirconia ceramics has been measured, and a broadening due to wall-collisions has been determined. The results are in agreement with similar measurements presented in [28] and theory presented in [11], which states that the wall-collision broadening can be added with the pressure broadening to give the total broadening due to intermolecular collisions and wall collisions.

The instrumentation for measuring on $O_2$ in scattering media has been improved by inserting a gas inlet that can be used to flush the pressure chamber with pure $O_2$, thereby increasing the strength of the absorption. The program for data acquisition has been improved with a function that automatically determines the number of averages that will give a good signal. An Allan deviation measurement has been performed on a sample of macroporous alumina, and it was found that the system could distinguish an absorption of around $3 \cdot 10^{-5}$, corresponding to an equivalent path length of 1.5 mm.

It has also been shown that the diffusion of $O_2$ out of polystyrene foam at low pressures is slow, and that the diffusion process can be described by an exponential equation. This experiment also shows that it is necessary to check that the diffusion of gas has ended before measuring the absorption in nanoporous materials. If the diffusion has not finished, higher pressure in the sample than in the ambient air will otherwise give a higher pressure broadening than expected, making it difficult to analyze the line shape of the absorption line.

A setup has been built to measure on $CO_2$ in scattering media. Measurements have been performed and it has been shown that it is possible to measure on $CO_2$ in scattering media. Better instrumentation, especially a better detector, is needed to be able to draw any conclusions about line broadening due to wall collisions in nanoporous materials.

A setup has also been built to measure on $H_2O$ in scattering materials. It has been shown to work, but the laser broke before any measurements could be performed.

## 9.2 Future work

It has been established that materials with smaller pore size give larger line broadening. Future work could include trying to find a relationship that would make it possible to measure the pore size from the line broadening of the absorption lines. Studying the line shape of the absorption line more in detail and seeing if it is possible to determine an expression that describes the absorption profile could also be attempted.

It would also be interesting to see if the line broadening is different for different gases. For that purpose, a new laser for measuring on $H_2O$ could be purchased. Also, a better detector for the $CO_2$ system could make analysis of the line shape easier. Then the wall-collision broadening of $O_2$, $H_2O$ and $CO_2$ could then be compared to see if there is a difference in the line broadening in the same sample. To further investigate the line-broadening effect, the systems for measuring on $CO_2$ and $H_2O$ should be modified to be able to measure at low pressures.

Another thing that should be performed is a measurement to determine the diffusion properties of $CO_2$ in the nanoporous samples. The diffusion of $H_2O$ and $O_2$ in the same sample of ceramics has been shown to be very different [13], and in order draw conclusions on the line-broadening of $CO_2$ absorption lines at low pressures, it is necessary to know how long it takes for the pressure to be the same in the entire sample.

# Bibliography


[1] M. Sjöholm, G. Somesfalean, J. Alnis, S. Andersson-Engels, and S. Svanberg. Analysis of gas dispersed in scattering media. *Optics Letters*, 26(1):16–18, 2001.

[2] J. Alnis, B. Anderson, M. Sjöholm, G. Somesfalean, and S. Svanberg. Laser spectroscopy of free molecular oxygen dispersed in wood materials. *Applied Physics B: Lasers and Optics*, 77:691–695, 2003.

[3] L. Persson, H. Gao, M. Sjöholm, and S. Svanberg. Diode laser absorption spectroscopy for studies of gas exchange in fruits. *Optics and Lasers, Engineering*, 44(7):687–698, 2006.

[4] M. Andersson, L. Persson, M. Sjöholm, and S. Svanberg. Spectroscopic studies of wood-drying processes. *Opt. Express*, 14(8):3641–3653, Apr 2006.

[5] L. Persson, M. Andersson, M. Cassel-Engquist, K. Svanberg, and S. Svanberg. Gas monitoring in human sinuses using tunable diode laser spectroscopy. *Journal of Biomedical Optics*, 12(5):054001, 2007.

[6] Anders Bruzelius. Sensing of free gas in human tissue with diode laser spectroscopy - Application to lung monitoring in premature neonates. Master's thesis, Lund Reports on Atomic Physics, LRAP-420, Lund University, 2010.

[7] M. Lewander, Z. Guan, L. Persson, A. Olsson, and S. Svanberg. Food monitoring based on diode laser gas spectroscopy. *Applied Physics B: Lasers and Optics*, 93:619–625, 2008.

[8] S. Svanberg. Optical analysis of trapped gas - Gas in scattering media absorption spectroscopy. *Laser Physics*, 20(1):68–77, 2010.

[9] R. H. Johnson and M. W. P. Strandberg. Broadening of microwave absorption lines by collisions with the cell walls. *Physical Review*, 86(5):811–812, 1952.

[10] M. Danos and S. Geschwind. Broadening of microwave absorption lines due to wall collisions. *Physical Review*, 91(5):1159–1162, 1953.

[11] S. C. M. Luijendijk. Effect of wall collisions on shape of microwave-absorption lines. *Journal of Physics B-atomic Molecular and Optical Physics*, 8(18):2995–3000, 1975.

[12] T. Svensson and Z. J. Shen. Laser spectroscopy of gas confined in nanoporous materials. *Applied Physics Letters*, 96(021107), 2010.

[13] T. Svensson, M. Lewander, and S. Svanberg. Laser absorption spectroscopy of water vapor confined in nanoporous alumina: Wall collision line broadening and gas diffusion dynamics. *Opt. Express*, 18(16):16460–16473, 2010.

[14] S. Svanberg. *Atomic and Molecular Spectroscopy: Basic Aspects and Practical Applications*. Springer, 4th edition, 2004.

[15] E. M. McCash C. N. Banwell. *Fundametals of Molecular Spectroscopy*. McGrawHill Book Company Europe, 4th edition, 1994.

[16] http://en.wikipedia.org/wiki/morse_potential.

[17] www.spectralcalc.com.

[18] D. S. Bomse, A. C. Stanton, and J. A. Silver. Frequency-modulation and wavelength modulation spectroscopies - Comparison of experimental methods using a lead-salt diode-laser. *Applied Optics*, 31(6):718–731, 1992.

[19] J. M. Suplee, E. A. Whittaker, and W. Lenth. Theoretical description of frequency-modulation and wavelength modulation spectroscopy. *Applied Optics*, 33(27):6294–6302, 1994.

[20] A. N. Dharams and A. M. Bullock. Applications of wavelength-modulation spectroscopy in resolution of pressure and modulation broadened spectra. *Applied Physics B: Lasers and Optics*, 63:283–292, 1996.

[21] B.E.A. Saleh and M.C. Teich. *Fundametals of Photonics*. Wiley, 2nd edition, 2007.

[22] S. Wang. Principles of distributed feedback and distributed Bragg-reflector lasers. *Journal of Quantum Electronics*, QE10(4):413–427, 1974.

[23] G. Somesfalean, M. Sjöholm, J. Alnis, C. af Klinteberg, S. Andersson-Engels, and S. Svanberg. Concentration measurement of gas embedded in scattering media by employing absorption and time-resolved laser spectroscopy. *Applied Optics*, 41(18):3538–3544, 2002.

[24] T. Svensson, E. Adolfsson, M. Lewander, and S. Svanberg. Disordered strongly scattering porous materials as miniature multipass cells. *arXiv*:1011.0900v1, 2010.

[25] Yu. N. Ponomarev, T. M. Petrova, A. M. Solodov, and A. A. Solodov. IR spectroscopy of water vapor confined in nanoporous silica aerogel. *Opt. Express*, 18(25):26062–26067, 2010.

[26] http://tf.nist.gov/general/glossary.htm.

[27] M.Sjöholm, L.Persson, and S.Svanberg. Gas diffusion measurements in porous media by the use of a laser spectroscopic technique. *Manuscript, presented in* [30].

[28] C. T. Xu, M. Lewander, S. Andersson-Engels, E. Adolfsson, T. Svensson, and S. Svanberg. Wall collision line broadening at reduced pressures: towards non-destructive characterization of nanoporous materials. *Manuscript, presented in* [31], 2010.

[29] T. Svensson, M. Andersson, L. Rippe, S. Svanberg, S. Andersson-Engels, J. Johansson, and S. Folestad. VCSEL-based oxygen spectroscopy for structural analysis of pharmaceutical solids. *Applied Physics B - Lasers and Optics*, 90(2):345–354, 2008.

[30] Mikael Sjöholm. *Laser Spectroscopy Analysis of Atmospheric Gases in Scattering Media*. PhD thesis, Lund Reports on atomic physics, LRAP-367, Lund University, 2006.

[31] Märta Lewander. *Laser Absorption Spectroscopy of Gas in Scattering Media*. PhD thesis, Lund Reports on atomic physics, LRAP-424, Lund University, 2010.